Lab - Mechatronics
Modelling and control of a Magnetic Levitation System

Tommaso Bocchietti 10740309
Daniele Cianca 10764733
Sara Orazzo 10995845

A.Y. 2024/25

POLITECNICO
MILANO 1863

We need to be consistent with the time used in the document. Present? Past? Future?

Contents

List of Figures

List of Tables

Listings

1 Introduction

This laboratory experience focuses on the precise control of the levitation of a ferromagnetic object within a magnetic field, a setup commonly known as a Magnetic Levitation System (MLS). The MLS represents a fascinating and challenging application of control theory, involving highly nonlinear dynamics and unstable equilibrium conditions.
The project has been structured into two main phases:

- **System modelling and identification**: in this phase, the system has been modelled by means of both differential equations and state space representation, and the parameters of the model have been identified through experimental data performed directly on the real system. Some preliminary consideration about stability and controllability has also been made.
- **Filters, estimators and controllers design**: in this phase, many control techniques have been implemented and tested. The main goal was to compare the performances of different controllers in terms of stability, robustness and tracking capabilities.

Report structure This report covers all the aspects of the laboratory experience, from the theoretical background to the practical implementation of the control algorithms. In particular, in Section 2 a brief introduction to the MLS is given, along with some high-level overview of the physical phenomena involved. In Section 3 the model of the system is derived, while in Section 4 the parameters of the model are identified through experimental data or collected from the datasheet. Section 5 is dedicated to the analysis of the model, focusing on stability and controllability. In Section 6 some filters and estimators are designed to reduce noise and improve the performances of the controllers designed in Section 7. Finally, in Section 9 some conclusions about the work done and possible future developments are drawn.

Tools An extensive use of `MATLAB` and `Simulink` has been made to implement the controllers and to simulate the system. All the source code and simulations used for this report can be found on the GitHub repository at the following link: `https://github.com/Bocchio01/062020-Lab-Mechatronics`.

2 Magnetic Levitation System

As stated in the introduction, the system under study is the Magnetic Levitation System (MLS) provided by `Inteco` [2]. In Figure 1 the system used in this work is shown.

Figure 1: Magnetic Levitation System. To be replaced by a photo taken by us.

As it can be seen quite clearly, the system is composed of a simple mechanical structure that is used to support two electromagnets and an optical infrared sensor. Along with the mechanical structure, a ferromagnetic ball and a control unit are present.
At its core principle, the system uses the interaction between the magnetic field generated by the electromagnets and the ferromagnetic ball to keep the ball in a desired position. The optical sensor is used to measure the position of the ball and provide feedback to the control unit that, in turn, adjusts the voltage applied to (and indeed the current flowing through) the electromagnets to keep the ball in a desired position. In Figure 2 a schematic representation of the upper half of the system is shown.

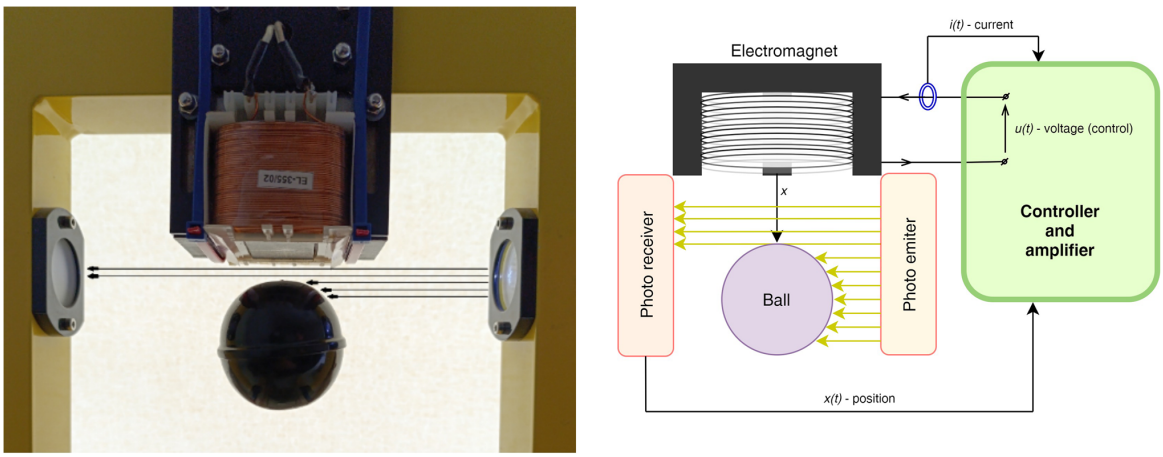

Figure 2: On the left, the infrared waves used to sense the ball position are represented by black arrows. On the right, a schematic representation of MLS is shown. One might also appreciate the feedback loop that is closed by the optical sensor. Credit to [3].

Real world application Magnetic levitation systems have diverse and transformative applications across various industries.

One of the most prominent uses is in high-speed transportation, such as MagLev trains, which achieve speeds exceeding $500km/h$ by eliminating wheel-rail friction. These systems offer smoother rides, reduced noise, and lower maintenance costs compared to traditional trains. Notable implementations include Japan's Chūō Shinkansen (see Figure 3a), aiming to connect Tokyo and Osaka, and China's $600km/h$ MagLev project, which demonstrates cutting-edge levitation control technology [6].
Other applications include microrobotics research, where magnetic levitation enables precise control of miniature robots for possible medical and industrial applications [7]. These robots can navigate complex environments, perform delicate tasks, and deliver targeted therapies with high precision and minimal invasiveness. Researchers are also exploring complex magnetic levitation environments for concurrent control of multiple robots, which could revolutionize microscale manufacturing and healthcare [4].
Additionally, scientific research benefits from these systems in experiments requiring vibration-free environments, such as advanced spectroscopy [1] and microgravity simulation [5].

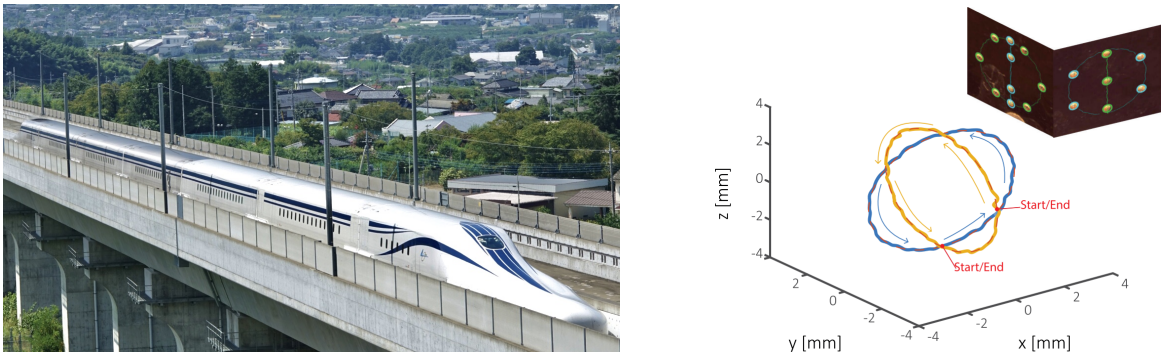

Figure 3: Applications of Magnetic Levitation. Japan's MagLev train Chūō Shinkansen [6] on the left, independent 3D control of a pair of microrobots via MLS techniques [4] on the right.

3 Modelling

The MLS is a complex system that can be divided into:

- **Electromagnetic subsystem**: it takes into account all the electrical components going from the power supply to the electromagnets themselves, and so the generation of the magnetic field by the coils;
- **Mechanical subsystem**: it takes into account the dynamics of the ball and the forces acting on it, including the electromagnetic forces generated by the magnetic field.

Due to the presence of the ball that moves inside a magnetic field, a complex connection between the two subsystems that goes beyond the simple force balance exists. For this reason, it's almost impossible to derive a complete model without considering both subsystems at the same time.
In Figure 4, a schematic representation of all the components of the system and the forces acting on it is shown. Instead, in Table 4 a brief description of the components is provided.

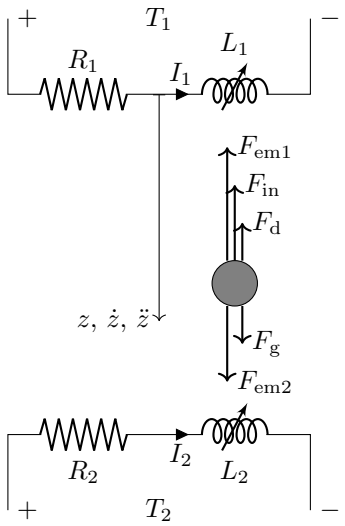

Name	Description	Units
F_{g}	Gravitational force	N
F_{in}	Inertial force	N
F_{d}	Drag force	N
$F_{\text{em1,2}}$	Electromagnetic forces	N
$R_{1,2}$	Resistances of the coils	Ω
$L_{1,2}$	Inductances of the coils	H
$I_{1,2}$	Currents flowing through the coils	A
$V_{1,2}$	Voltages applied to the coils	V
$T_{1,2}$	Temperatures of the coils	$°C$

Figure 4: Schematic representation of the MLS system and description of its components.

In the following sections, we will derive the equations that governs the MLS system, adopting an energetic approach that starts from the energy conservation principle.

3.1 Mathematical model

We can now proceed with the derivation of the equations that govern the system.
At first, we can recall the energy conservation principle stating that the sum of the kinetic, potential, and dissipated energy of the system is equivalent to the work done by the external forces acting on it.

3.1.1 Lagrangian formulation

Thanks to Lagrange's equation we encapsulate the energy conservation principle by writing the following:

$$\frac{d}{dt}\left(\frac{\partial \mathcal{T}}{\partial \dot{\mathbf{u}}}\right) - \frac{\partial \mathcal{T}}{\partial \mathbf{u}} + \frac{\partial \mathcal{D}}{\partial \dot{\mathbf{u}}} + \frac{\partial \mathcal{U}}{\partial \mathbf{u}} = \mathcal{Q} \tag{1}$$

Where $\mathbf{u}$ is the generalized coordinates of the system, $\mathbf{T}$ is the kinetic energy, $\mathbf{D}$ is the dissipated one, $\mathbf{U}$ is the potential energy, and $\mathbf{Q}$ is the generalized input to the system.
At first, we can give a definition of all the energetic terms included in Equation 1 for the MLS system. Notice that with respect to traditional purely mechanical systems, we also have to consider the stored energy in the coils as inductors, the dissipation due to the resistance of the coils, and the potential energy given by the external power supply.
By doing so, we can write the kinetic energy of the system as:

$$\mathcal{T} = \frac{1}{2}m\dot{z}^2 + \frac{1}{2}L_1(z, \dot{q_1}, T_1)\dot{q_1}^2 + \frac{1}{2}L_2(z, \dot{q_2}, T_2)\dot{q_2}^2 \tag{2}$$

Where m is the mass of the ball, L_1 and L_2 are the inductances of the coils, and q_1 and q_2 are the charges stored in the coils. It follows that $\dot{q_1}$ and $\dot{q_2}$ are the currents flowing through the coils.
The dissipated energy of the system can be written as:

$$\mathcal{D} = \int_{\dot{z}(\cdot)} \frac{1}{2} C_d A \rho \dot{z}^2 d\dot{z} + \int_{\dot{q_1}(\cdot)} R_1(\dot{q_1}, T_1) \dot{q_1} d\dot{q_1} + \int_{\dot{q_2}(\cdot)} R_2(\dot{q_2}, T_2) \dot{q_2} d\dot{q_2} \tag{3}$$

Where C_d is the drag coefficient for a generic spherical object, A is the cross-sectional area of the ball, and ρ is the density of air.
Instead, the potential energy of the system can be written as:

$$\mathcal{U} = -mgz - q_1 V_1 - q_2 V_2 \tag{4}$$

Where V_1 and V_2 are the voltages applied to the coils.
Finally, the generalized input to the system can be evaluated as:

$$\mathcal{Q} = 0 \tag{5}$$

For convenience, we have chosen to consider both the external power supplied and the gravitational force as potential energy terms and not as generalized inputs. Notice also the minus sign in the gravitational potential energy term, which is due to the fact that the gravitational force tends to increase the potential energy with respect to the chosen reference frame (positive downwards, see Figure 4).

3.1.2 Electrical components model

Before proceeding, it's necessary to explicitly state the dependence of the inductance and resistance terms on the generalized coordinates of the system.
We can assume that, in first approximation, the sensitivity of both the electrical components to the temperature of the coils is negligible. This is strong and possibly incorrect assumption, but it allows us to simplify the model and focus on the main dynamics of the system.

Resistance model For what regards the resistance terms, we can assume that the resistance of the coils is constant and so does not depend on neither the current flowing through them nor the temperature of the coils. Under these assumptions, we can write the resistance terms as:

$$\begin{aligned} R_1 &= R_1(\dot{q_1}, T_1) = R_{10} \\ R_2 &= R_2(\dot{q_2}, T_2) = R_{20} \end{aligned} \tag{6}$$

Where R_{*0} are the resistances of the coils measured at ambient temperature with negligible current flowing through them.

Inductance model Considering the inductance terms, we will again neglect the dependence on the coil's temperature, but we will take into account the variation of the inductance due to the presence of the ball in the magnetic field (principal source of nonlinearity in the system) and also the dependence over the current flowing through the coils. For the assumption stated above, we will model the inductance terms as:

$$\begin{aligned} L_1 &= L_1(z, \dot{q_1}, T_1) = L_{10} + L_{1z} e^{-a_{1z} z} + L_{1I} * \arctan(a_{1I} I_1 - b_{1I}) \\ L_2 &= L_2(z, \dot{q_2}, T_2) = L_{20} + L_{2z} e^{-a_{2z}(h-2r-z)} + L_{2I} * \arctan(a_{2I} I_2 - b_{2I}) \end{aligned} \tag{7}$$

Where L_{*0} are the nominal inductances values. Instead, L_{*z}, a_{*z} and L_{*I}, a_{*I}, b_{*I} are coefficients that take into account the variation of the inductance due to the presence of the ball in the magnetic field and the current flowing through the coils, respectively.
It has to be noted that this model was suggested by a careful analysis of experimental data and is not directly based on theoretical considerations. Some previous models of inductance can also be found in the literature, but they are often too complex and not suitable for control purposes.

3.1.3 Equations of motion

Considering the assumptions made in both the resistance and inductance models (Equations 6, 7) to neglect their dependence on the temperature of the coils, we can see that the generalized coordinates are z, q_1, and q_2, and so the vector of generalized coordinates is $\mathbf{u} = [z, q_1, q_2]^T$.
Once $\mathbf{u}$ has been identified, the procedure to derive the equations of motion is straightforward. Based on Equation 1, we can write the following system of equations:

$$\begin{cases} \frac{d}{dt}\left(\frac{\partial \mathcal{T}}{\partial \dot{z}}\right) - \frac{\partial \mathcal{T}}{\partial z} + \frac{\partial \mathcal{D}}{\partial \dot{z}} + \frac{\partial \mathcal{U}}{\partial z} = \mathcal{Q} \\ \frac{d}{dt}\left(\frac{\partial \mathcal{T}}{\partial \dot{q_1}}\right) - \frac{\partial \mathcal{T}}{\partial q_1} + \frac{\partial \mathcal{D}}{\partial \dot{q_1}} + \frac{\partial \mathcal{U}}{\partial q_1} = \mathcal{Q} \\ \frac{d}{dt}\left(\frac{\partial \mathcal{T}}{\partial \dot{q_2}}\right) - \frac{\partial \mathcal{T}}{\partial q_2} + \frac{\partial \mathcal{D}}{\partial \dot{q_2}} + \frac{\partial \mathcal{U}}{\partial q_2} = \mathcal{Q} \end{cases} \tag{8}$$

By substituting the energetic terms obtained in Equations 2, 3, 4, 5 into the set of equations above, we obtain the following equations of motion:

$$\begin{cases} m\ddot{z} - \frac{1}{2}\frac{\partial L_1}{\partial z}\dot{q_1}^2 - \frac{1}{2}\frac{\partial L_2}{\partial z}\dot{q_2}^2 + \frac{1}{2}C_d A\rho \dot{z}|\dot{z}| - mg = 0 \\ \frac{1}{2}\left(\frac{\partial^2 L_1}{\partial \dot{q_1}\partial z}\dot{z} + \frac{\partial^2 L_1}{\partial \dot{q_1}^2}\ddot{q_1}\right)\dot{q_1}^2 + \frac{\partial L_1}{\partial \dot{q_1}}\dot{q_1}\ddot{q_1} + \left(\frac{\partial L_1}{\partial z}\dot{z} + \frac{\partial L_1}{\partial \dot{q_1}}\ddot{q_1}\right)\dot{q_1} + L_1\ddot{q_1} + R_1\dot{q_1} - V_1 = 0 \\ \frac{1}{2}\left(\frac{\partial^2 L_2}{\partial \dot{q_2}\partial z}\dot{z} + \frac{\partial^2 L_2}{\partial \dot{q_2}^2}\ddot{q_2}\right)\dot{q_2}^2 + \frac{\partial L_2}{\partial \dot{q_2}}\dot{q_2}\ddot{q_2} + \left(\frac{\partial L_2}{\partial z}\dot{z} + \frac{\partial L_2}{\partial \dot{q_2}}\ddot{q_2}\right)\dot{q_2} + L_2\ddot{q_2} + R_2\dot{q_2} - V_2 = 0 \end{cases} \tag{9}$$

For convenience, we can replace time derivatives of charges leveraging the definition of current as the time derivative of the charge. Moreover, we can group the terms in the equations above so to move derivatives with respect to the generalized coordinates on the left-hand side of the equations. Finally, we also transform the second order differential equations into first order differential equations by introducing a fourth equation and considering the ball velocity v as a state variable. By doing so, we obtain the following set of equations:

$$\begin{cases} \dot{z} = v \\ \dot{v} = m^{-1}\left(\frac{1}{2}\frac{\partial L_1}{\partial z}I_1^2 + \frac{1}{2}\frac{\partial L_2}{\partial z}I_2^2 - \frac{1}{2}C_d A\rho\dot{z}|\dot{z}| + mg\right) \\ \dot{I_1} = \left(\frac{1}{2}\frac{\partial^2 L_1}{\partial I_1^2}I_1^2 + 2\frac{\partial L_1}{\partial I_1}I_1 + L_1\right)^{-1}\left(-\frac{1}{2}\frac{\partial^2 L_1}{\partial I_1 \partial z}\dot{z}I_1^2 - \frac{\partial L_1}{\partial z}\dot{z}I_1 - R_1 I_1 + V_1\right) = 0 \\ \dot{I_2} = \left(\frac{1}{2}\frac{\partial^2 L_2}{\partial I_2^2}I_2^2 + 2\frac{\partial L_2}{\partial I_2}I_2 + L_2\right)^{-1}\left(-\frac{1}{2}\frac{\partial^2 L_2}{\partial I_2 \partial z}\dot{z}I_2^2 - \frac{\partial L_2}{\partial z}\dot{z}I_2 - R_2 I_2 + V_2\right) = 0 \end{cases} \tag{10}$$

The set of equations above represents the complete mathematical model of the MLS system.

3.1.4 Model reduction

In order to simplify the model and make it more suitable for control purposes, we can make some assumptions that allow us to reduce the complexity of the system without losing its main dynamics.
Based also on the experimental data collected during the parameters' identification phase (Section 4), we can state that the sensitivity of the inductance terms to the current flowing through the coils is negligible around the operating point. Moreover, also the velocity of the ball will always be small, and so every term that is linearly dependent on it can be neglected. Based on these assumptions, we can impose the following conditions to the system:

$$\begin{cases} \frac{\partial L_*}{\partial I_*} & \approx 0 \\ \frac{\partial^2 L_*}{\partial I_*^2} & \approx 0 \\ \dot{z} & \approx 0 \end{cases} \tag{11}$$

Equations of motion 10 consequently simplify to:

$$\begin{cases} \dot{z} = v \\ \dot{v} = m^{-1}\left(\frac{1}{2}\frac{\partial L_1}{\partial z}I_1^2 + \frac{1}{2}\frac{\partial L_2}{\partial z}I_2^2 + mg\right) \\ \dot{I_1} = L_1^{-1}\left(-R_1 I_1 + V_1\right) \\ \dot{I_2} = L_2^{-1}\left(-R_2 I_2 + V_2\right) \end{cases} \tag{12}$$

3.1.5 Control input correction

A final important remark has to be made about the input given to the system.
So far, in all the equations above, we have considered the input to the system as the voltage applied to the coils. However, the actual input to the system is the duty cycle of the PWM[1] signal that drives the coils.
Ideally, the relationship between the duty cycle and the voltage applied to the coils is a direct proportionality, but in practice, a linear approximation must be made. One can easily see that by simply connecting the power supply to the coils, a minimum voltage will be applied and a certain amount of current will flow through. In the following, we will refer to this current and voltage as I_{*min} and V_{*min} respectively. In the context of control purposes, these zones where it's not possible to have a direct control over the applied voltage are called *black zones*.

[1] Pulse-Width Modulation

Under these considerations, one can rewrite the voltages applied to the coils V_* as a function of the duty cycle U_* as a piece wise linear function:

$$V_* = \begin{cases} k_* U_* + c_* & \text{if } U_* \geq U_{*min} \\ V_{*min} & \text{if } U_* < U_{*min} \end{cases} \tag{13}$$

Where k_* and c_* are the slope and the intercept of the linear relation, respectively, and U_{*min} is the minimum duty cycle that allows to move outside the black zone and have a direct control over the voltage applied to the coils.
By substituting the voltages in the set of Equations 12, we obtain the final set of equations that govern the system:

$$\begin{cases} \dot{z} = v \\ \dot{v} = m^{-1} \left(\frac{1}{2} \frac{\partial L_1}{\partial z} I_1^2 + \frac{1}{2} \frac{\partial L_2}{\partial z} I_2^2 + mg \right) \\ \dot{I}_1 = L_1^{-1} \left(-R_1 I_1 + (k_1 U_1 + c_1) \right) \\ \dot{I}_2 = L_2^{-1} \left(-R_2 I_2 + (k_2 U_2 + c_2) \right) \end{cases} \tag{14}$$

3.2 Model Linearization

The model derived in the previous subsections (Equations 14) is highly non-linear. In order to be able to apply linear control techniques, it is necessary to linearize the model around a given operating point.

3.2.1 Operating point computation

The operating point is the set of values of the state and input around which the linearization is performed.
Given the set of Equations 14, the operating point can be computed by setting the time derivatives to zero, set at least 2 of the state variables or input variables to constant values and solve the remaining equations. Based on their physical meaning, it's reasonable to set the position of the ball z and the current in the lower electromagnet I_2. By doing so, all the other state and input variables can be computed by solving the following set of equations:

$$\mathbf{x}_{op} = \begin{bmatrix} z_{op} \\ v_{op} \\ I_{1op} \\ I_{2op} \end{bmatrix} = \begin{cases} z^* \\ 0 \\ \sqrt{-(2mg + \frac{\partial L_2}{\partial z}\big|_{z_{op}} I_{2op}^2) / \frac{\partial L_1}{\partial z}\big|_{z_{op}}} \\ I_2^* \end{cases} \tag{15}$$

$$\mathbf{u}_{op} = \begin{bmatrix} U_{1op} \\ U_{2op} \end{bmatrix} = \begin{cases} \max\left[0, R_{10} \left(I_{1op} - I_{1min} \right) / k_1 \right] \\ \max\left[0, R_{20} \left(I_{2op} - I_{2min} \right) / k_2 \right] \end{cases} \tag{16}$$

Where z^* is the desired position of the ball and I_2^* is the desired current in the lower electromagnet. As we can see, once those values are set, all the other states and inputs can be computed uniquely.

3.2.2 Linearized model derivation

Based on the operating point computed in the previous subsection, the linearized model can be obtained by performing a Taylor expansion around the operating point up to the first order terms of Equations 14 or Equations 55.
Before performing the linearization, we briefly recall the general form of a Taylor expansion of a function $f(\mathbf{x})$ around a point $\mathbf{x}_{op}$:

$$f(\mathbf{x}) \approx f(\mathbf{x}_{op}) + \nabla f(\mathbf{x}_{op}) \cdot (\mathbf{x} - \mathbf{x}_{op}) \tag{17}$$

Where $\nabla f(\mathbf{x}_{op})$ is the gradient of $f(\mathbf{x})$ evaluated at $\mathbf{x}_{op}$.
By applying the Taylor expansion to the non-linear model, the linearized model can be obtained as:

$$\mathbf{f}(\mathbf{x}) - \mathbf{f}(\mathbf{x}_{op}) \approx \left. \frac{\partial \mathbf{f}}{\partial \mathbf{x}} \right|_{\mathbf{x}_{op}} \cdot (\mathbf{x} - \mathbf{x}_{op}) \tag{18}$$

Considering now the set of Equations 14, the linearized model can be obtained as:

Solve this formatting issue. Split the equation multiple lines?

$$\begin{cases} \dot{z} - \dot{z_{op}} & \approx 1(v - v_{op}) \\ \dot{v} - \dot{v_{op}} & \approx m^{-1} \left(\frac{1}{2}\frac{\partial^2 L_1}{\partial z^2}\Big|_{\mathbf{x}_{op}} (z - z_{op}) I_{1op}^2 + \frac{1}{2}\frac{\partial^2 L_2}{\partial z^2}\Big|_{\mathbf{x}_{op}} (z - z_{op}) I_{2op}^2 + \frac{\partial L_1}{\partial z}\Big|_{\mathbf{x}_{op}} I_{1op}(I_1 - I_{1op}) + \frac{\partial L_2}{\partial z}\Big|_{\mathbf{x}_{op}} I_{2op}(I_2 - I_{2op}) \right) \\ \dot{I_1} - \dot{I_{1op}} & \approx \left(-L_1^{-2}\frac{\partial L_1}{\partial z}\left(-R_1 I_1 + k_1 U_1 + c_1\right)\right)\Big|_{\mathbf{x}_{op}} (z - z_{op}) + \left(-L_1^{-1} R_1\right)\Big|_{\mathbf{x}_{op}} (I_1 - I_{1op}) + \left(L_1^{-1} k_1\right)\Big|_{\mathbf{x}_{op}} (U_1 - U_{1op}) \\ \dot{I_2} - \dot{I_{2op}} & \approx \left(-L_2^{-2}\frac{\partial L_2}{\partial z}\left(-R_2 I_2 + k_2 U_2 + c_2\right)\right)\Big|_{\mathbf{x}_{op}} (z - z_{op}) + \left(-L_2^{-1} R_2\right)\Big|_{\mathbf{x}_{op}} (I_2 - I_{2op}) + \left(L_2^{-1} k_2\right)\Big|_{\mathbf{x}_{op}} (U_2 - U_{2op}) \end{cases} \tag{19}$$

Notice that also during the linearization process, the model has been simplified by reapplying the assumptions made in the set of Equations 11.

3.3 State Space Representation

In the optics of control theory, it is useful to represent the system in the state space form. The state space representation is a mathematical model of a physical system as a set of input, output and state variables related by first-order differential equations. The state space representation is particularly useful for linear systems, as it allows to easily apply linear control techniques.
A generic nonlinear system can be represented in the state space form as:

$$\begin{aligned} \dot{\mathbf{x}} &= f(\mathbf{x}, \mathbf{u}) \\ \mathbf{y} &= g(\mathbf{x}, \mathbf{u}) \end{aligned} \tag{20}$$

Where $\mathbf{x}$ is the state vector and $\mathbf{u}$ is the input vector, while f and g are generic functions that describe the system dynamics and the output equations, respectively.
Similarly to what has been done in the previous subsection, we can perform a linearization of the system around an operating point to obtain the linearized state space representation in the form of:

$$\begin{aligned} \dot{\delta\mathbf{x}} &\approx A\delta\mathbf{x} + B\delta\mathbf{u} \\ \delta\mathbf{y} &\approx C\delta\mathbf{x} + D\delta\mathbf{u} \end{aligned} \tag{21}$$

Where $\delta\mathbf{x}$ and $\delta\mathbf{u}$ are the deviations of the state and input vectors from the operating point, respectively. Instead, A, B, C and D are the Jacobian matrices with respect to the state and input vectors evaluated at the operating point.

MLS state space representation Given the linearized model derived in the previous subsection (Equation 19), we can define the state vector $\mathbf{x}$ and the input vector $\mathbf{u}$ as:

$$\mathbf{x} = \begin{bmatrix} z \\ v \\ I_1 \\ I_2 \end{bmatrix} \quad \mathbf{u} = \begin{bmatrix} U_1 \\ U_2 \end{bmatrix} \tag{22}$$

Once the state and input vectors have been defined, the linearized state space representation can be obtained by leveraging the linearized model derived previously. The matrices A, B, C and D are then defined as:

$$\begin{aligned} A &= \frac{\partial f}{\partial \mathbf{x}}\Big|_{(\mathbf{x}_{op}, \mathbf{u}_{op})} = \begin{bmatrix} 0 & 1 & 0 & 0 \\ a_{21} & 0 & a_{23} & a_{24} \\ a_{31} & 0 & a_{33} & 0 \\ a_{41} & 0 & 0 & a_{44} \end{bmatrix} \\ B &= \frac{\partial f}{\partial \mathbf{u}}\Big|_{(\mathbf{x}_{op}, \mathbf{u}_{op})} = \begin{bmatrix} 0 & 0 \\ 0 & 0 \\ b_{31} & 0 \\ 0 & b_{42} \end{bmatrix} \\ C &= \frac{\partial g}{\partial \mathbf{x}}\Big|_{(\mathbf{x}_{op}, \mathbf{u}_{op})} = \begin{bmatrix} 1 & 0 & 0 & 0 \end{bmatrix} \\ D &= \frac{\partial g}{\partial \mathbf{u}}\Big|_{(\mathbf{x}_{op}, \mathbf{u}_{op})} = \begin{bmatrix} 0 & 0 \end{bmatrix} \end{aligned} \tag{23}$$

Based on Equation 19, the elements of the matrices A, B, C and D can be computed as:

$$
\begin{aligned}
a_{21} &= \frac{1}{m}\left(\frac{1}{2}\frac{\partial^2 L_1}{\partial z^2}I_1^2 + \frac{1}{2}\frac{\partial^2 L_2}{\partial z^2}I_2^2\right)\Big|_{(\mathbf{x}_{op},\mathbf{u}_{op})} \\
a_{23} &= \frac{1}{m}\left(\frac{\partial L_1}{\partial z}I_1\right)\Big|_{(\mathbf{x}_{op},\mathbf{u}_{op})} \\
a_{24} &= \frac{1}{m}\left(\frac{\partial L_2}{\partial z}I_2\right)\Big|_{(\mathbf{x}_{op},\mathbf{u}_{op})} \\
a_{31} &= \left(-L_1^{-2}\frac{\partial L_1}{\partial z}\left(-R_1 I_1 + k_1 U_1 + c_1\right)\right)\Big|_{(\mathbf{x}_{op},\mathbf{u}_{op})} \\
a_{33} &= \left(L_1^{-1}(-R_1)\right)\big|_{(\mathbf{x}_{op},\mathbf{u}_{op})} \\
a_{41} &= \left(-L_2^{-2}\frac{\partial L_2}{\partial z}\left(-R_2 I_2 + k_2 U_2 + c_2\right)\right)\Big|_{(\mathbf{x}_{op},\mathbf{u}_{op})} \\
a_{44} &= \left(L_2^{-1}(-R_2)\right)\big|_{(\mathbf{x}_{op},\mathbf{u}_{op})} \\
b_{31} &= \left(L_1^{-1}k_1\right)\big|_{(\mathbf{x}_{op},\mathbf{u}_{op})} \\
b_{42} &= \left(L_2^{-1}k_2\right)\big|_{(\mathbf{x}_{op},\mathbf{u}_{op})}
\end{aligned}
\tag{24}
$$

Is the output equation correct? Because in the end we want to control z, but in output from the MagLev we receive all the states...

3.4 Single Coil Configuration

In this section, we will present the model of the MLS system when only the upper coil is used for control purposes. This configuration is the one that will be used in the rest of the document and the laboratory activities. The choice has been taken in order to deal with a simpler SISO system, which is easier to control and analyze.
In the following, starting from Equation 14, we will at derive the reduced model, linearize it and represent it in state-space form.

Reduced Equations of Motion At first, if we consider energizing only the upper coil, we can simply remove the terms related to the lower coil from the equations of motion. Based on Equation 14, we can write the following equations:

$$
\begin{cases}
\dot{z} = v \\
\dot{v} = m^{-1}\left(\frac{1}{2}\frac{\partial L_1}{\partial z}I_1^2 + mg\right) \\
\dot{I}_1 = L_1^{-1}\left(-R_1 I_1 + (k_1 U_1 + c_1)\right)
\end{cases}
\tag{25}
$$

Linearization As already discussed in Section 3.2, we can linearize via Taylor expansion the equations of motion around one of its operating points. For the case of the single coil configuration, Equations 15 and 16 reduce to:

$$
\mathbf{x}_{op} = \begin{bmatrix} z_{op} \\ v_{op} \\ I_{1op} \end{bmatrix} = \begin{cases} z^* \\ 0 \\ \sqrt{-(2mg)/\frac{\partial L_1}{\partial z}\big|_{z_{op}}} \end{cases}
\tag{26}
$$

$$
\mathbf{u}_{op} = \begin{bmatrix} U_{1op} \end{bmatrix} = \left\{ \max\left[0, R_{10}\left(I_{1op} - I_{1min}\right)/k_1\right] \right.
\tag{27}
$$

By performing the Taylor expansion of Equations 25 around the operating point, we obtain the following linearized model:

$$\begin{cases} \dot{z} - \dot{z_{op}} & \approx 1(v - v_{op}) \\ \dot{v} - \dot{v_{op}} & \approx m^{-1} \left(\frac{1}{2} \frac{\partial^2 L_1}{\partial z^2} \Big|_{\mathbf{x}_{op}} (z - z_{op}) I_{1op}^2 + \frac{\partial L_1}{\partial z} \Big|_{\mathbf{x}_{op}} I_{1op}(I_1 - I_{1op}) \right) \\ \dot{I_1} - \dot{I_{1op}} & \approx \left(-L_1^{-2} \frac{\partial L_1}{\partial z} \left(-R_1 I_1 + k_1 U_1 + c_1\right)\right) \Big|_{\mathbf{x}_{op}} (z - z_{op}) + \left(-L_1^{-1} R_1\right) \Big|_{\mathbf{x}_{op}} (I_1 - I_{1op}) + \left(L_1^{-1} k_1\right) \Big|_{\mathbf{x}_{op}} (U_1 - U_{1op}) \end{cases} \tag{28}$$

State-Space Representation Finally, we can represent the linearized model in state-space form. Given the reduction of the system to a SISO one, we need to redefine the state vector $\mathbf{x}$ and the input vector $\mathbf{u}$ as follows:

$$\mathbf{x} = \begin{bmatrix} z \\ v \\ I_1 \end{bmatrix} \quad \mathbf{u} = \begin{bmatrix} U_1 \end{bmatrix} \tag{29}$$

Once the state and input vectors have been defined, the linearized state-space representation can be obtained by leveraging the linearized model derived previously. The matrices A, B, C and D are then defined as:

$$\begin{aligned} A &= \frac{\partial f}{\partial \mathbf{x}} \Big|_{(\mathbf{x}_{op}, \mathbf{u}_{op})} = \begin{bmatrix} 0 & 1 & 0 \\ a_{21} & 0 & a_{23} \\ a_{31} & 0 & a_{33} \end{bmatrix} \\ B &= \frac{\partial f}{\partial \mathbf{u}} \Big|_{(\mathbf{x}_{op}, \mathbf{u}_{op})} = \begin{bmatrix} 0 \\ 0 \\ b_{31} \end{bmatrix} \\ C &= \frac{\partial g}{\partial \mathbf{x}} \Big|_{(\mathbf{x}_{op}, \mathbf{u}_{op})} = \begin{bmatrix} 1 & 0 & 0 \end{bmatrix} \\ D &= \frac{\partial g}{\partial \mathbf{u}} \Big|_{(\mathbf{x}_{op}, \mathbf{u}_{op})} = \begin{bmatrix} 0 \end{bmatrix} \end{aligned} \tag{30}$$

Given the unboundedness between the two coils currents, the elements of the matrices A, B, C and D remain exactly as already computed in Section 24.

4 Identification

To effectively control the system, it is crucial to identify its physical and dynamic parameters. This process involves a series of carefully designed experiments and measurements to extract reliable data.
The parameter identification process is divided into the following steps:

1. **Direct measurement**: using conventional instruments, measure physical parameters that do not require specific test setups, such as geometric dimensions or mass or static resistance of the coils.
2. **Sensor characterization**: map the relationship between the ball's position and the output voltage of the infrared sensor. Additionally, statistically analyze the output of the sensors used internally to estimate the system state.
3. **Control-to-voltage dependency**: examine the relationship between the control signal and the resulting applied voltage to the coils ($V = V(U)$).
4. **Inductance characterization**: determine parameters for inductances based on the model described in Equations 7. This involves analyzing the system's electrical response under various conditions.
5. **Force validation**: measure the electromagnetic force applied to the ball to validate both the identified parameters and the overall model's accuracy.

Except for direct measurements, all tests are performed using the data acquisition capabilities of the `Inteco` control unit itself.
To simplify the identification process, we will assume the lower and upper coils have identical parameters unless explicitly stated otherwise. This assumption allows us to streamline both the methodology and the notation by avoiding subscripts that distinguish the two coils.
In all subsequent tests, parameters are identified using measurements from the upper coil.

4.1 Direct measurement

Many of the parameters of the system can be directly measured using a scale, a caliper or a voltmeter.
Among those, we have the mass of the ball m, the radius of the ball r, the distance between the upper and lower coils h and the resistance of the coil R. Their values are reported in Table 1.

Parameter	Value	Units
g	9.81	m/s^2
m	0.06157	kg
r	0.06125/2	m
h	0.098	m
R_0	4.17	Ω

Table 1: Directly measured parameters and constants

4.2 Sensors characterization

In this subsection, we will focus on the characterization of the sensors used internally by the control unit to measure or estimate the system state.

4.2.1 Voltage to position mapping

At first, we need to create the mapping between the voltage output of the infrared sensor and the position of the ball. To do so, we simply sample the output voltage of the infrared sensor and the position of the ball using the data acquisition system included in the `Inteco` control unit and a caliper.
The obtained data is shown in Figure 5.

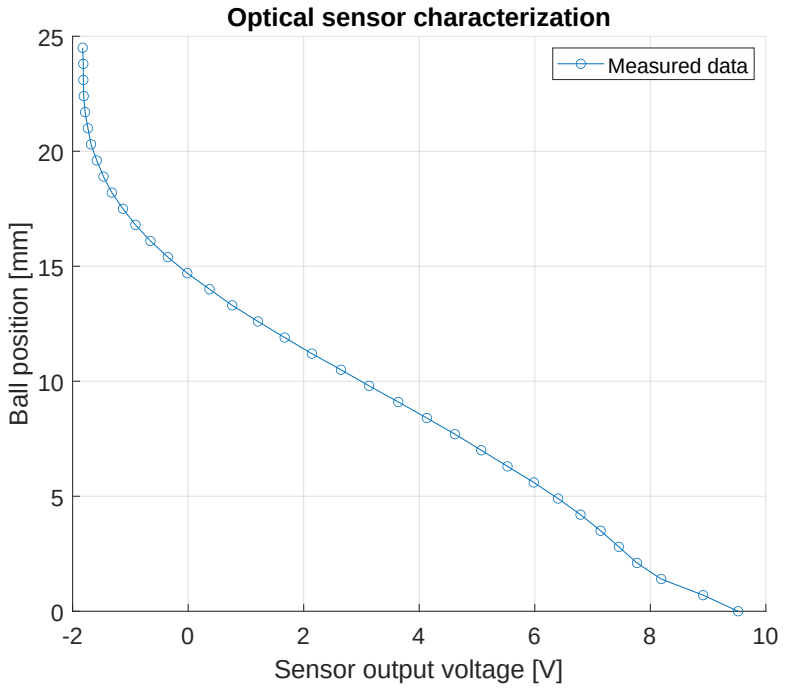

Figure 5: Position of the ball as a function of the output voltage of the infrared optical sensor.

One can clearly see the non-linear relationship between the ball's position and the output voltage of the infrared sensor.
Moreover, it's important to underline the hardware limitations of the sensor that allows a maximum measurement distance of $\approx 20[mm]$ from the upper coil before reaching its saturation limit.

4.2.2 Sensors noise analysis

A comprehensive analysis of the sensors' noise is crucial to correctly estimate both the position of the ball and the coils' current. The experimental setup consists of keeping the ball at a fixed position and recording the sensors' output for a certain amount of time imposing a zero control signal. The analysis then assumes the sensors' noise to be a zero-mean Gaussian white noise process.
With this optics, we can estimate the standard deviation for each sensor and use it to design the filters and estimators in the following sections (see Section 6).

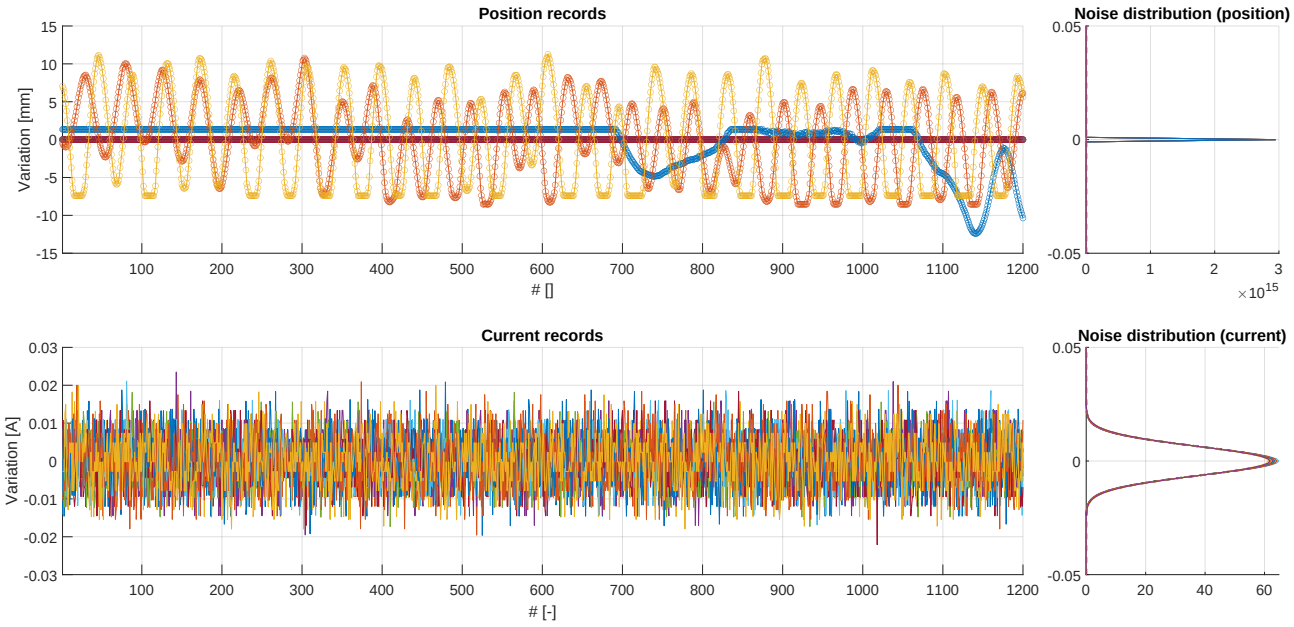

Figure 6: Sensors' noise analysis. Repeat the test inside the infrared sensor saturation limit.

In Figure 6, the analysis of the sensors' noise is shown.

The left plots show the time history of the sensor output variations, while the right plots show the Gaussian distribution of the sensors' noise with the mean distribution marked with a dashed black line. The upper plots refer to the infrared sensor, while the lower plots refer to the current sensor.
The standard deviation and covariance of the sensors' noise is reported in Table 2.

Sensor	Standard deviation	Covariance
Infrared	$1.402804 \cdot 10^{-3}$ $[m]$	$7.166031 \cdot 10^{-6}$ $[m^2]$
Current	$6.327979 \cdot 10^{-3}$ $[A]$	$4.005490 \cdot 10^{-5}$ $[A^2]$

Table 2: Standard deviation and covariance of the sensors' noise.

4.3 Control to voltage

As already clarified in Section 3.1.5, what we actually control is the duty cycle of the PWM signal that is applied to the coils. However, as we saw in Equation 12, the model consider the effective voltage applied to the coils as input.
In order to use the control signal as input to the model, we need to identify the parameters of the relation between the control signal and the effective voltage applied to the coils which has already been discussed in Equation 13.
The experimental procedure to identify this relation can be summarized in the following steps:

1. Connect the control unit to the coils and to the power supply.
2. Connect the multimeter to the coils and set it to measure the voltage.
3. Set the control unit to a specific duty cycle.
4. Measure the voltage applied to the coils.
5. Repeat steps 3 and 4 for many duty cycles.

The output of this test is a series of points that can be fitted to 13 in order to identify the parameters of the relation. In Figure 7 we can observe both the measured points, the linear fitting and the effective voltage applied considering also the initial black zone.

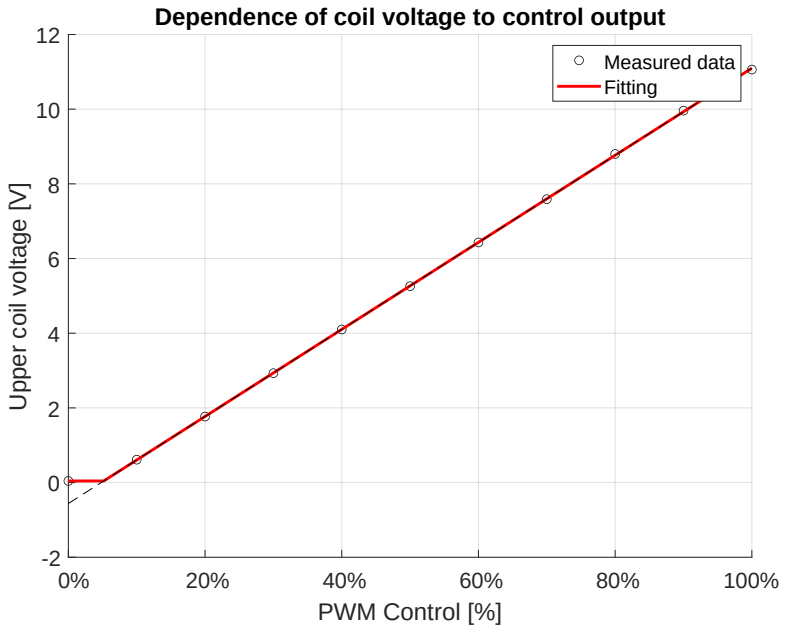

Figure 7: Control to voltage identification

As we can see, the linear model for the relation $V = f(U) = f(\text{PWM})$ is a good approximation outside the initial black zone control.
The values of the parameters for the Equation 13 are shown in Table 3. One might refer to Section 3.1.5 for an explanation of the parameters.

Parameter	Value	Units
V_{min}	$4.300000 \cdot 10^{-2}$	V
U_{min}	5.179276	%
k	$1.165800 \cdot 10^{1}$	$V/\%$
c	$-5.608000 \cdot 10^{-1}$	V

Table 3: Control to voltage identification parameters

4.4 Inductances characterization

A key parameter of the system is the inductance of the coils.
As already proposed in Equation 7, the inductance of the coils cannot be considered constant and both its dependence on the current and the position of the ball must be taken into account when dealing with the MLS. In order to identify the inductance of the coils and all the parameters needed to characterize them, we have to measure $L(z, I)$ for many currents and ball positions. Once these values are known, we can fit the data to the model proposed in Equation 7 and identify its parameters.
Given a certain (fix in time) position of the ball and a certain current step input, we can measure the value of the inductance of the coils, knowing that:

$$V = RI + \frac{d(LI)}{dt} = RI + \left(\frac{\partial L}{\partial I} I + L\right) \dot{I} \tag{31}$$

If we suppose for a moment that the variation of the inductance with the current is negligible, we can obtain a closed form solution for the current in the RL circuit as follows:

$$I(t) = \frac{V_{final}}{R_0} \left(1 - e^{-\frac{R_0}{L} t}\right) \tag{32}$$

Given the previous equations, we can adopt the following strategy to fully characterize the inductance of the coils over the range of possible ball positions and currents:

1. Fix the ball at a certain height (z^*);
2. Apply a certain current step input to the system (I^*);
3. Measure the current in the coils ($I(t)$);
4. Fit the measured current to the model proposed in Equation 32 and identify $L(z^*, I^*)$;
5. Repeat from step 2 for different step inputs of currents;
6. Repeat from step 1 for different ball positions.

In Figure 8 we can see on the left all the experimental data representing the dynamics of the current in the coils for different step inputs of currents and different ball positions, while on the right we can see the fitting of some experimental data to the model proposed in Equation 32.

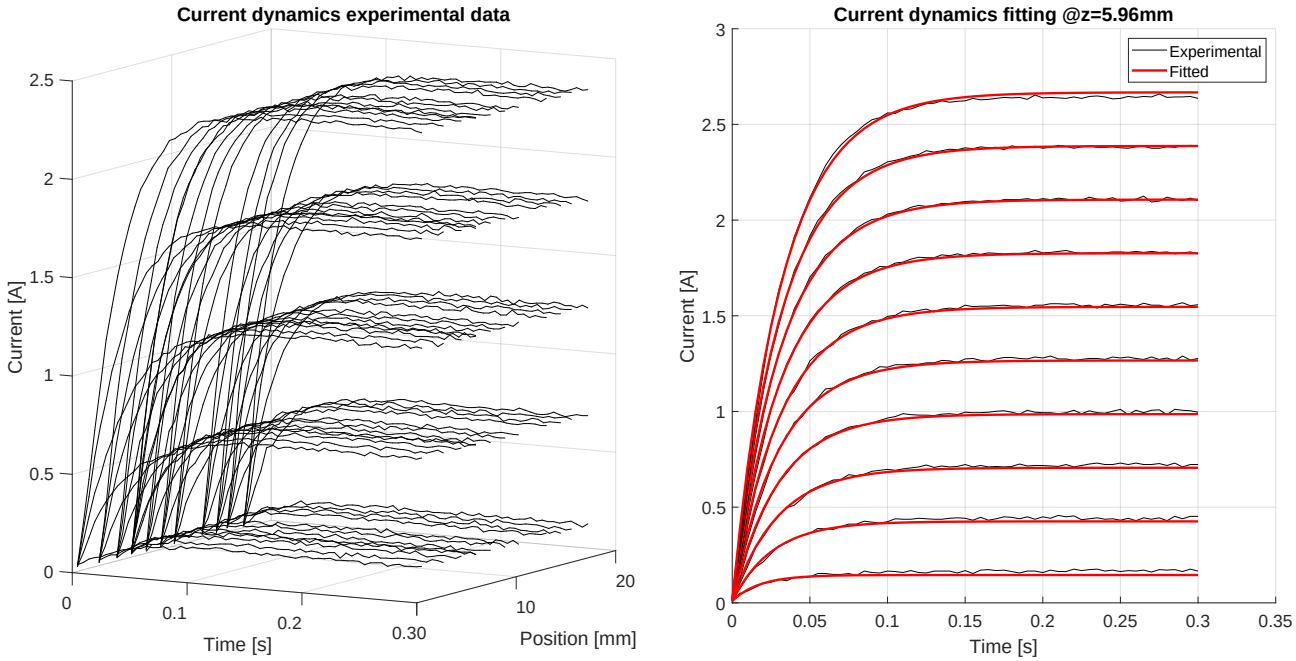

Figure 8: Inductance characterization for different currents and ball positions

From the right side of Figure 8 we can see that the fitting of the data to the model proposed in Equation 32 is optimal for middle values of the current, while it tends to underestimate and overestimate the current for low and high values of the current, respectively. This behavior is probably due to the fact that the variation of the inductance with the current that has been neglected in the model of the current (Equation 32) is not negligible and should have been taken into account.
Thanks to the data obtained from the multiple tests, we can now fit the values of the inductance of the coils to the model proposed in Equation 7 and identify its parameters. The obtained model fitting is shown in Figure 9.

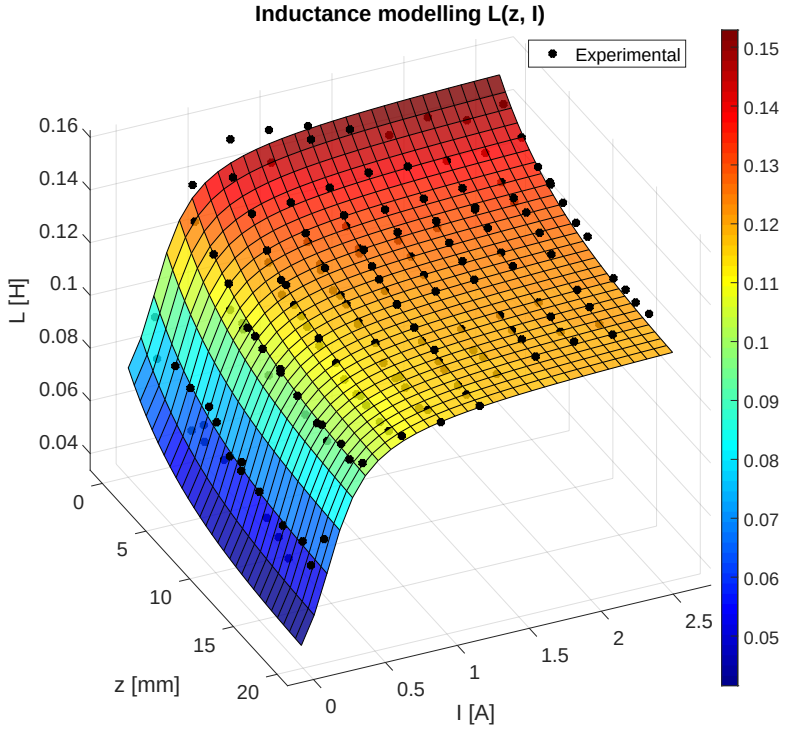

Figure 9: Inductance model fitting

The 210 black dots in Figure 9 represent the experimental data obtained from the fitting of currents dynamics for different current steps and ball positions.
The values of the parameters are shown in Table 4.

Parameter	Value	Units
L_0	$6.122809 \cdot 10^{-2}$	H
a_z	$1.837302 \cdot 10^{+2}$	$1/m$
L_z	$3.438228 \cdot 10^{-2}$	H
a_I	$4.759750 \cdot 10^{+0}$	
b_I	$6.704755 \cdot 10^{-1}$	A
L_I	$3.831209 \cdot 10^{-2}$	H

Table 4: Inductance characterization parameters

As a double check against the model proposed in Equation 7, one can also observe the R squared value of the fitting $R^2 = 0.961$, which is a good indicator of the quality of the fitting.

4.5 Force validation

Finally, we can proceed with the force validation test.
Thanks to the data obtained from the previous tests, we are already able to predict the force applied to the ball by the inductance. In particular, we already know that the electromagnetic force applied to the ball is given by the following equation:

$$F_{em} = \frac{1}{2}\frac{\partial L}{\partial z} I^2 = \frac{1}{2}(-a_z L_z e^{-a_z z}) I^2 \tag{33}$$

Because of the previously identified parameters, we have an analytical expression for the sensitivity of the inductance with respect to the position of the ball. However, due to uncertainties in the identification of the parameters, we can expect some discrepancies between the predicted force and the measured one.
In order to quantify these discrepancies and validate the model, we use a direct method to measure the force applied to the ball by the inductance and compare it with the predicted one. To do so, we recall Equation 14 and in particular the equation relative to $\dot{v}$:

$$\dot{v} = m^{-1}\left(\frac{1}{2}\frac{\partial L_1}{\partial z} I_1^2 + \frac{1}{2}\frac{\partial L_2}{\partial z} I_2^2 + mg\right) \tag{34}$$

If we consider the system at rest or equivalently at the incipient motion of the ball, we can simplify the equation as follows:

$$0 = \frac{1}{2}\frac{\partial L_1}{\partial z} I_1^2 + \frac{1}{2}\frac{\partial L_2}{\partial z} I_2^2 + mg \tag{35}$$

Supposing now that only the first coil is energized, we can further simplify the equation as follows:

$$0 = \frac{1}{2}\frac{\partial L_1}{\partial z} I_1^2 + mg \tag{36}$$

Which leads to:

$$\frac{\partial L_1}{\partial z} = -2\frac{mg}{I_1^2} \tag{37}$$

This last equation basically tells us that in steady state conditions, when the ball is levitating (i.e. $\dot{z} = 0$ and not supported by any platform), the sensitivity of the inductance of the first coil has an analytical expression that can be directly evaluated by measuring the current in the first coil and the position of the ball.
In order to follow this approach, the experimental steps are as follows:

1. By regulating a lower platform, the ball is placed at a certain height (z^*);
2. A linearly increasing voltage is applied to the first coil;
3. The current circulating in the first coil is measured;
4. The current at which the ball starts to levitate is identified;
5. The sensitivity of the inductance is calculated using Equation 37.
6. The test is repeated for different initial positions of the ball.

In Figure 10 we can see both the position of the ball (red line) and the current circulating in the first coil (black line) around the identified levitation point (marked by the vertical black dashed line).

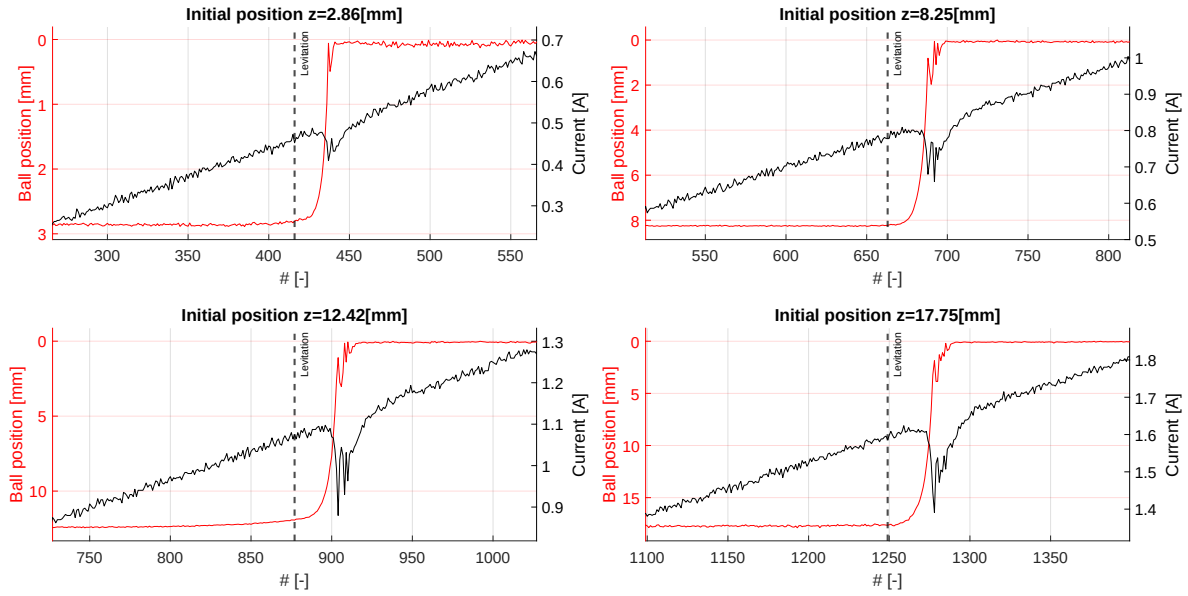

Figure 10: Position of the ball and current in the first coil around the levitation point (marked by vertical black dashed line)

Instead, in Figure 11, we can observe both the measured data and the fitted ones. On the right side figure, a complete characterization of the electromagnetic force has been reconstructed based again on the above equations.

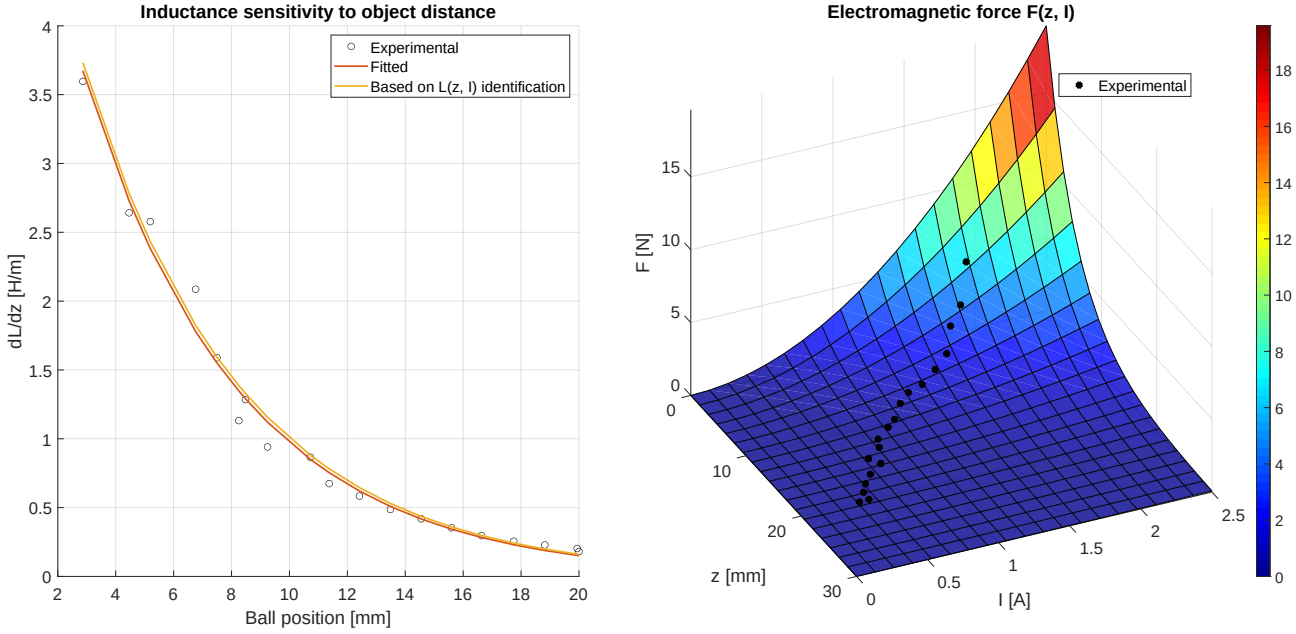

Figure 11: Dynamic inductance characteristics and electromagnet force

The left-hand side of Figure 11 shows a comparison between the measured data (black circles), their fitting (red line) and the sensitivity of the inductance coming from the parameters identified in Section 4.4 (yellow line). Data shows great accuracy in almost the entire range of the ball position.
The right-hand side of Figure 11 shows the electromagnetic force generated by the first coil as a function of both the ball position and the current circulating in the coil. One can notice that the force has an exponential behavior with respect to the ball position and a quadratic behavior with respect to the current.

5 Model Analysis

Given the model derived in Section 3 and the parameters identified in Section 4, we can now proceed with the analysis of the system.
As we have already discussed, the governing equations of the MLS are strongly non-linear. In order to analyze the stability of the system, we linearize the model around the operating point and derive the state-space representation of the linearized model as already discussed in Section 3.4.
For the successive analysis, we consider the following operating point:

$$\mathbf{x}_{op} = \begin{bmatrix} z_{op} \\ v_{op} \\ I_{1op} \end{bmatrix} = \begin{cases} z^* = 10 \cdot 10^{-3} \\ v^* = 0 \\ \sqrt{-(2mg)/\frac{\partial L_1}{\partial z}\big|_{z_{op}}} \approx 1.087 \end{cases} \tag{38}$$

$$\mathbf{u}_{op} = \begin{bmatrix} U_{1op} \end{bmatrix} = \left\{ \max\left[0, R_{10}\left(I_{1op} - I_{1min}\right)/k_1\right] \approx 0.380 \right. \tag{39}$$

At these conditions, the system matrices A, B, C and D are given as follows:

$$A = \begin{bmatrix} 0 & 1 & 0 \\ 1802 & 0 & -18.06 \\ -47.29 & 0 & -35.19 \end{bmatrix} \quad B = \begin{bmatrix} 0 \\ 0 \\ 98.37 \end{bmatrix} \tag{40}$$

$$C = \begin{bmatrix} 1 & 0 & 0 \end{bmatrix} \quad D = \begin{bmatrix} 0 \end{bmatrix} \tag{41}$$

5.1 Controllability and observability

The controllability and observability of the system are crucial aspects to consider when designing a control strategy. Controllability ensures that the system's state can be manipulated by the control inputs, while observability guarantees that the state can be accurately estimated from the system's outputs.
The controllability matrix $\mathcal{KR}$ and observability matrix $\mathcal{KO}$ are defined as follows:

$$\begin{aligned} \mathcal{KR} &= \begin{bmatrix} B & AB & A^2B \end{bmatrix} \\ \mathcal{KO} &= \begin{bmatrix} C^T & (CA)^T & (CA^2)^T \end{bmatrix} \end{aligned} \tag{42}$$

By computing the rank of the controllability and observability matrices, we can determine whether the system is controllable and observable. In particular, based on the Kalman's reachability and observability conditions, the system is controllable if and only if $\text{rank}(\mathcal{KR}) = n$ and observable if and only if $\text{rank}(\mathcal{KO}) = n$, where n is the number of states in the system.
An explicit computation shows that the system is both controllable and observable, given that:

$$\mathcal{KR} = 10^5 \begin{bmatrix} 0 & 0 & -0.0178 \\ 0 & -0.0178 & 0.6250 \\ 0.0010 & -0.0346 & 1.2180 \end{bmatrix} \quad \mathcal{KO} = 10^3 \begin{bmatrix} 0.0010 & 0 & 0 \\ 0 & 0.0010 & 0 \\ 1.8025 & 0 & -0.0181 \end{bmatrix} \tag{43}$$

5.2 Open loop stability

The stability of the system can be assessed by analyzing the poles of the open-loop system, which corresponds to the eigenvalues of the system matrix A. By solving the characteristic equation $\det(sI - A) = 0$, we find that the poles of the system are located at:

$$\lambda = \begin{cases} 42.5848 \\ -40.5300 \\ -37.2420 \end{cases} \tag{44}$$

One can clearly notice that one of the poles is located on the right-hand side of the complex plane, indicating that the system is inherently unstable.
By plotting the poles and zeros of the system in the complex plane, we obtain the pole-zero map shown in Figure 12.

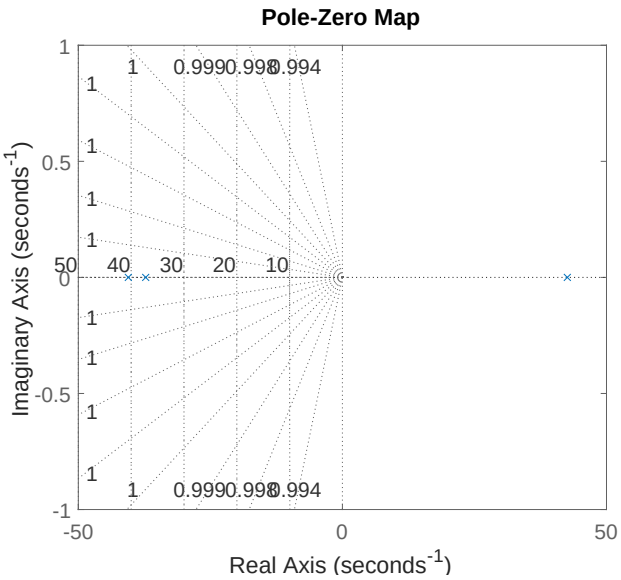

Figure 12: Pole-Zero Map

Notice that the system doesn't have any zeros, and as previously mentioned, one of the poles is located in the right-hand side of the complex plane, confirming the system's instability.

Root Locus Considering the unstable nature of the system, we perform a root locus analysis to identify potential gains that achieve a stable closed-loop system. The root locus plot is shown in Figure 13.

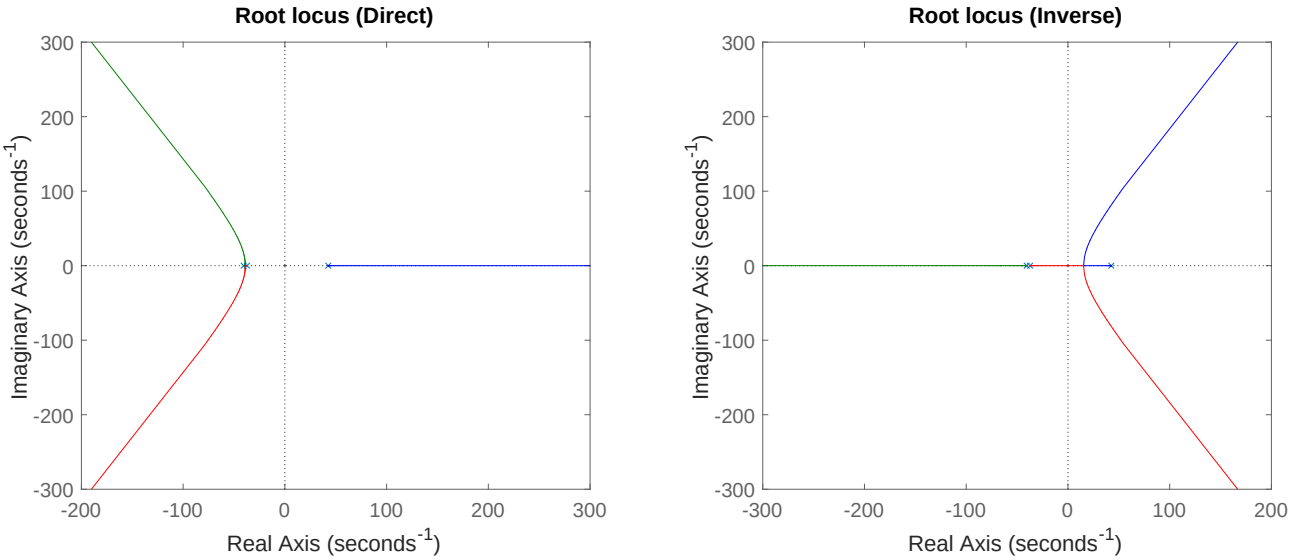

Figure 13: Root Locus Plot

The root locus plot illustrates how the system poles migrate in the complex plane as the proportional gain of the controller is varied.
Again, we observe that one the three poles is unstable. Moreover, we also notice that a simple proportional controller is not sufficient to stabilize the system, as the poles do not move to the left-hand side of the complex plane for any value of the gain K.

Bode Diagram To further analyze the stability of the system, we consider the Bode plot for the open-loop transfer function. The Bode diagram is shown in Figure 14.

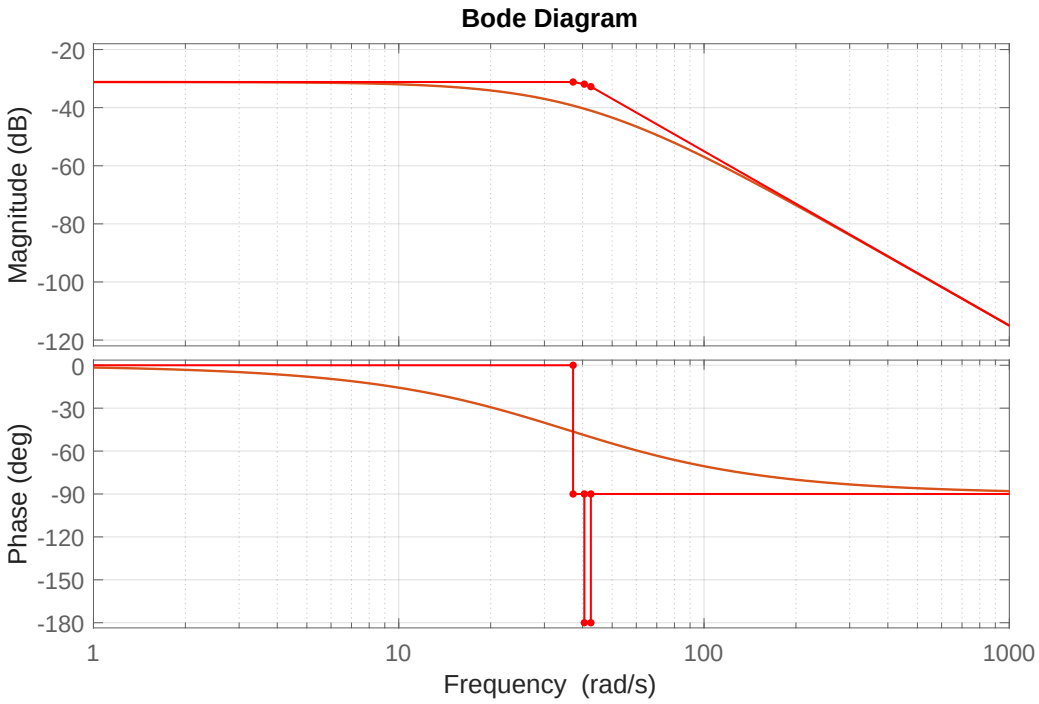

Figure 14: Bode Plot

Again, we observe that the system is unstable, as the gain margin is negative and the phase margin is less than $-180°$.

6 Filters & Estimators Design

In this section, we will design filters and estimators to be used in the control loop of the MLS. The main goal of these filters and estimators is to reduce the noise present in the sensors' measurements and to estimate the states of the system that are not directly measurable.
In particular, we will design a low-pass filter, a Luenberger observer, a Kalman filter, and an Extended Kalman filter.

6.1 Low Pass Filter

To be checked. Not sure about the correctness of the calculations and the estimation of the natural frequency of the system.
The low pass filter is a filter that allows the low frequency components of a signal to pass through, while attenuating the high frequency components. By correctly choosing the cut-off frequency of the filter, it's possible to remove the noise from the signal, while preserving the useful information.
The transfer function of a first order low pass filter is given by:

$$G(s) = \frac{1}{\tau s + 1} \tag{45}$$

Where τ is the time constant of the filter, and it's related to the cut-off frequency ω_c by the relation $\tau = \frac{1}{\omega_c}$.

Filter on position From the `Inteco` manual, we have understood that the vertical velocity of the ball is computed via numerical discretization of the position. This also means that the noise present in the position measurement is amplified by the differentiation process. To reduce this noise, we design a low pass filter to be applied to the position measurements before the differentiation.
In order to estimate the cut-off frequency of the filter, one can either perform a spectral decomposition of the signal to obtain the maximum frequency present in the signal, or estimate (via experiments on the real system) the natural frequency of the system and choose a cut-off frequency accordingly.
From preliminary tests, we have observed the ball reaches maximum speeds of around $v_{max} \approx 0.3 m/s$. Therefore, we can roughly the period of the ball to be around $T_p = 2\frac{(h-2r)}{v_{max}} \approx 0.245 s$. From this, we can estimate the natural frequency of the system to be:

$$\omega_n = \frac{2\pi}{T_p} \approx 25 rad/s \tag{46}$$

As rule of thumb, we could choose the cut-off frequency to be one decade after the natural frequency, i.e. $\omega_c = 10\omega_n \approx 250 rad/s$.
However, we know that the smaller the cut-off frequency, the better the noise attenuation. On the other hand, the smaller the cut-off frequency, the larger the phase lag introduced by the filter.
As a compromise between noise attenuation and phase lag, we choose the cut-off frequency to be $\omega_c = 200 rad/s$. By doing so, we obtain the time constant of the filter to be $\tau = \frac{1}{200} = 5ms$ and a corresponding phase delay introduced by the filter of:

$$\phi = -\arctan(\omega_n \tau) = -\arctan(25 \cdot 5 \cdot 10^{-3}) \approx -7.1^\circ \tag{47}$$

Filter on current The current measurement is also affected by noise. However, based on experiments, we have observed that even a slight delay in the current measurement can lead to instability of the system. Therefore, we choose not to apply a low pass filter to the current measurements.

6.2 Luenberger Observer

The Luenberger observer is a state observer that allows to estimate the state of a system, given the input coming from the controllers and at least one measured output. The observer is designed in such a way that the error between the estimated state and the real state converges to zero, as time goes to infinity.
To do so, one can consider the following dynamical system:

$$\begin{cases} \dot{\hat{x}} = A\hat{x} + Bu + L(y - C\hat{x}) \\ \hat{y} = C\hat{x} \end{cases} \tag{48}$$

Where $\hat{x}$ is the estimated state, $\hat{y}$ is the estimated output, L is the observer gain, and y is the measured output of the system.

The poles of the observer are given by the eigenvalues of the matrix $A - LC$, and the observer is stable if the poles are placed in the left half plane of the complex plane.
The observer gain L can be computed using the Ackermann formula, which is a generalization of the pole placement method for state-space systems.

Design Given that there are no restrictions (except for being in the left-hand side of the complex plane) for the position of the poles, we choose by chance the followings:

$$eig(A - LC) = \begin{bmatrix} ?? \\ ?? \\ ?? \end{bmatrix} \tag{49}$$

6.3 Kalman Filter

The Kalman Filter is a powerful algorithm used for estimating the state of a dynamic system from a series of noisy measurements. It is widely used in control systems, robotics, signal processing, and navigation due to its ability to provide real-time, optimal state estimates by considering system dynamics and measurement noise.
The filter operates in two main steps: the prediction step, which estimates the current state based on the system model, and the update step, which refines this estimate using new measurement data.
Mathematically, the filter assumes a linear system model of the form:

$$\begin{aligned} \dot{x} &= Ax + Bu + w \\ y &= Cx + Du + v \end{aligned} \tag{50}$$

Where x is the state vector, u is the control input, y is the measurement, A is the state transition matrix, B is the control input matrix, C is the observation matrix, and w and v are process and measurement noise, respectively. Among the assumptions of the Kalman filter, both the process and measurement noise are assumed to be zero-mean Gaussian white noise with known covariances Q and R.
One of the key strengths of the Kalman Filter is its ability to provide smooth state estimates, even in the presence of high measurement noise, without introducing delays. This makes it critical for real-time applications such as tracking, navigation (e.g., GPS), and autonomous systems. Additionally, it assumes the noise covariances $Q = \text{Cov}(w_k)$ and $R = \text{Cov}(v_k)$ are known, which helps in calculating the Kalman gain:

$$K = P^- H^T (HP^- H^T + R)^{-1} \tag{51}$$

Where P_k^- is the predicted estimate covariance.
Once the Kalman gain is calculated, the filter proceeds to the update step, where it corrects the predicted state estimate based on the measurement. To do so, the same structure seen already in the Luenberger observer is used (Equation 48), but with the Kalman gain instead of the observer gain. This reads:

$$\begin{cases} \dot{\hat{x}} = A\hat{x} + Bu + K(y - C\hat{x}) \\ \hat{y} = C\hat{x} \end{cases} \tag{52}$$

Design As we have already seen in the Luenberger observer design, the poles of the observer are given by the eigenvalues of the matrix $A - KC$, and the observer is stable if the poles are placed in the left half plane of the complex plane. The Kalman gain K can be computed using Equation 51.
By doing so, we obtain the following K matrix:

$$K = \begin{bmatrix} ?? \\ ?? \\ ?? \end{bmatrix} \tag{53}$$

6.4 Extended Kalman Filter

7 Controllers Design

We need to state clearly that we are not using the lower electromagnets for control purposes.
In this section, we move onto the design of the controllers that will be used to control the system.
As we have clarified in the previous modelling section (Section 3), the system is highly nonlinear with respect to both position and current, and we control it by acting on the input PWM signal.
In the following, we will present three main families of controllers that have been adopted for the control of the system:

- **PID Controllers**: a simple controller that uses the error signal, its history and derivative to compute the control signal (Section 7.1)
- **LQR Controllers**: a controller that minimizes a quadratic cost function to compute the control signal (Section 7.2)
- **MPC Controllers**: a controller that predicts the future evolution of the system and computes the control signal by minimizing a cost function (Section 7.3)

For each of these controllers, we will briefly present their theoretical background and the design choices that have been made.
Results and comparisons between the different controllers will be presented in the next section (Section 8).

7.1 PID Controllers

The Proportional-Integral-Derivative (PID) controller is a simple controller that uses the error signal, its history and derivative to compute the control signal. It is a widely used controller in industry due to its simplicity and effectiveness in many applications.
The PID controller is defined by the following equation:

$$u(t) = K_p e(t) + K_i \int_0^t e(\tau)dt + K_d \frac{de(t)}{dt} = K_p \left(e(t) + \frac{1}{T_i} \int_0^t e(\tau)dt + T_d \frac{de(t)}{dt} \right) \tag{54}$$

Where K_p, K_i and K_d are the proportional, integral and derivative gains, respectively. T_i and T_d instead are the integral and derivative time constants, respectively.

7.1.1 PID classic

In its simplest form, the PID is a linear controller whose three gains are tuned based on the linearization of the system.

7.1.2 PID with Anti-Windup correction

7.1.3 PID with gain scheduling

7.2 LQ Controllers

7.2.1 LQR

7.2.2 LQR with tracking capabilities

7.2.3 LQI

7.3 MPC Controllers

7.3.1 MPC with linear model

Test	Filter	Controller	Reference
1	Low Pass or Kalman (?)	PID anti wind-up	[square, sine]
2	Low Pass or Kalman (?)	PID gain scheduling	[square, sine]
3	Low Pass or Kalman (?)	LQR tracking	[square, sine]
4	Low Pass or Kalman (?)	LQI	[square, sine]
5	Low Pass or Kalman (?)	MPC	[square, sine]
6	Luenderberger	[PID gain scheduling, LQI]	sine
7	Kalman	[PID gain scheduling, LQI]	sine
8	Extended Kalman	[PID gain scheduling, LQI]	sine

Table 5: Tests to be performed

8 Results

Total of 8*2 = 16 tests to be performed.
First 5*2 to compare the controllers, then 3*2 to compare the estimators.
Here goes all the results obtained from the different tests. Keeping all the results in this section will make it easier to compare the different controllers and estimators.

9 Conclusions

In this work, we have presented the modelling and control of a Magnetic Levitation System (MLS). The system is composed of two electromagnets, a ferromagnetic ball and a control unit. The goal of the system is to levitate the ball at a certain height, by controlling the current in the electromagnets.
At first, a complete model of the system has been derived, followed by the identification of its parameters. Then, filters and estimators have been designed to estimate the state of the system, given the input and the output signals. Finally, controllers have been designed to control the position of the ball.
The results show that the designed controllers are able to stabilize the system, and to track the desired position of the ball. All the controllers proved to be robust to noise and model uncertainties.
In conclusion, the system has been successfully modelled and controlled, and the designed controllers are able to stabilize the system and to track the desired position of the ball.
Future work could include the design of a more advanced controller, such as Feedback Linearization or Backstepping controllers, to further improve the performance of the system in highly dynamic conditions.

References

[1] Shencheng Ge, Alex Nemiroski, Katherine A. Mirica, Charles R. Mace, Jonathan W. Hennek, Ashok A. Kumar, and George M. Whitesides. Magnetic levitation in chemistry, materials science, and biochemistry. *Angewandte Chemie International Edition*, 59(41):17810–17855, 2020.

[2] INTECO. Magnetic levitation systems — inteco. `https://www.inteco.com.pl/products/magnetic-levitation-systems/`, 2014. [Online; accessed 26-September-2024].

[3] Marcin Jastrzebski and Jacek Kabzinski. Adaptive control of magnetic levitation system based on fuzzy inversion. *Scientific Reports*, 14(1):24815, Oct 2024.

[4] Federico Ongaro, Stefano Pane, Stefano Scheggi, and Sarthak Misra. Design of an electromagnetic setup for independent three-dimensional control of pairs of identical and nonidentical microrobots. *IEEE transactions on robotics*, 35(1):174–183, February 2019.

[5] Hamid Sanavandi and Wei Guo. A magnetic levitation based low-gravity simulator with an unprecedented large functional volume. *npj Microgravity*, 7(1):40, Oct 2021.

[6] Wikipedia contributors. Scmaglev — Wikipedia, the free encyclopedia. `https://en.wikipedia.org/w/index.php?title=SCMaglev&oldid=1243224393`, 2024. [Online; accessed 28-September-2024].

[7] Tiantian Xu, Jiangfan Yu, Xiaohui Yan, Hongsoo Choi, and Li Zhang. Magnetic actuation based motion control for microrobots: An overview. *Micromachines*, 6(9):1346–1364, 2015.

A Literature model

In the literature, the model of the MLS system is often further simplified by considering empirical values associated with the inductances and resistances of the coils. In particular, from the `Inteco` manual, the following set of equations is reported:

$$\begin{cases} \dot{z} = v \\ \dot{v} = m^{-1}\left(-F_{em1} + F_{em2} + mg\right) \\ \dot{I}_1 = \frac{1}{f(z)}\left(-I_1 + kiU_1 + ci\right) \\ \dot{I}_2 = \frac{1}{f(h-2r-z)}\left(-I_2 + kiU_2 + ci\right) \end{cases} \tag{55}$$

Where $f(x)$ is an empirical function that takes into account the variation of the inductances due to the presence of the ball in the magnetic field and has the following form:

$$f(z) = \frac{f_{IP1}}{f_{IP2}} e^{\left(-\frac{z}{f_{IP2}}\right)} \tag{56}$$

While F_{em1} and F_{em2} are the electromagnetic forces acting on the ball and have the following form:

$$\begin{cases} F_{em1} &= \frac{F_{emP1}}{F_{emP2}} e^{-\frac{z}{F_{emP2}}} I_1^2 \\ F_{em2} &= \frac{F_{emP1}}{F_{emP2}} e^{-\frac{h-2r-z}{F_{emP2}}} I_2^2 \end{cases} \tag{57}$$

Also from literature, and in particular from the datasheet of the `Inteco` control unit, we can retrieve the following values about the literature model proposed in Equation 55:

Parameter	**Value**	**Units**
F_{emP1}	$1.7521 \cdot 10^{-2}$	H
F_{emP2}	$5.8231 \cdot 10^{-3}$	m
f_{iP1}	$1.4142 \cdot 10^{-4}$	$m \cdot s$
f_{iP2}	$4.5626 \cdot 10^{-3}$	m
c_i	0.0243	A
k_i	2.5165	A

Table 6: Literature parameters